Inter-modal four-wave mixing study in a two-mode fiber

S. M. M. Friis,[1,2,*] I. Begleris,[1] Y. Jung,[1] K. Rottwitt,[2] P. Petropoulos,[1] D. J. Richardson,[1] P. Horak,[1] and F. Parmigiani[1,3]

[1]*Optoelectronics Research Centre, University of Southampton, SO17 1BJ, United Kingdom*
[2]*Department of Photonics Engineering, Technical University of Denmark, 2800 Kongens Lyngby, Denmark*
[3]*frp@orc.soton.ac.uk*
[*]*smmf@fotonik.dtu.dk*

Abstract: We demonstrate efficient four-wave mixing among different spatial modes in a 1-km long two-mode fiber at telecommunication wavelengths. Two pumps excite the LP_{01} and LP_{11} modes, respectively, while the probe signal excites the LP_{01} mode, and the phase conjugation (PC) and Bragg scattering (BS) idlers are generated in the LP_{11} mode. For these processes we experimentally characterize their phase matching efficiency and bandwidth and find that they depend critically on the wavelength separation of the two pumps, in good agreement with the numerical study we carried out. We also confirm experimentally that BS has a larger bandwidth than PC for the optimum choice of the pump wavelength separation.

OCIS codes: (060.2330) Fiber optics communications; (070.4340) Nonlinear optical signal processing; (190.4380) Nonlinear optics, four-wave mixing.

References and links

1. R. H. Stolen, J. E. Bjorkholm, and A. Ashkin, "Phase-matched three-wave mixing in silica fiber optical waveguides," Appl. Phys. Lett. **24,** 308–310 (1974).
2. L. Grüner-Nielsen, Y. Sun, J. W. Nicholson, D. Jakobsen, K. G. Jespersen, R. Lingle, and B. Pálsdóttir, "Few mode transmission fiber with low DGD, low mode coupling, and low loss," J. Lightwave Technol. **30,** 3693–3698 (2012).
3. R.-J. Essiambre, M. A. Mestre, R. Ryf, A. H. Gnauck, R. W. Tkach, A. R. Chraplyvy, Y. Sun, X. Jiang, and R. Lingle, Jr., "Experimental observation of inter-modal cross-phase modulation in few-mode fibers," IEEE Photon. Technol. Lett. **25,** 535–538 (2013).
4. R.-J. Essiambre, M. A. Mestre, R. Ryf, A. H. Gnauck, R. W. Tkach, A. R. Chraplyvy, Y. Sun, X. Jiang, and R. Lingle, Jr., "Experimental investigation of inter-modal four-wave mixing in few-mode fibers," IEEE Photon. Technol. Lett. **25,** 539–542 (2013).
5. M. Schnack, T. Hellwig, M. Brinkmann, and C. Fallnich, "Ultrafast two-color all-optical transverse mode conversion in a graded-index fiber," Opt. Lett. **40,** 4675–4678 (2015).
6. S. Radic, "Parametric amplification and processing in optical fibers," Laser Photon. Rev. **2,** 498–513 (2008).
7. J. Hansryd, P. A. Andrekson, M. Westlund, J. Li, and P. Hedekvist, "Fiber-based optical parametric amplifiers and their applications," IEEE J. Sel. Top. Quantum Electron. **8**, 506–520 (2002).
8. F. Yaman, Q. Lin, and G. P. Agrawal, "Fiber optic parametric amplifiers for lightwave systems," in *Guided Wave Optical Components and Devices,* B. P. Pal, ed. (Academic, 2006).
9. Z. Tong, A. Bogris, M. Karlsson, and P. A. Andrekson, "Raman-induced asymmetric pump noise transfer in fiber-optical parametric amplifiers," IEEE Photon. Technol. Lett. **22,** 386–388 (2010).
10. S. M. M. Friis, K. Rottwitt, and C. J. McKinstrie, "Raman and loss induced quantum noise in depleted fiber optical parametric amplifiers," Opt. Express **21,** 29320–29331 (2013).
11. Z. Tong, A. Bogris, M. Karlsson, and P. A. Andrekson, "Full characterization of the signal and idler noise figure spectra in single-pumped fiber optical parametric amplifiers," Opt. Express **18**, 2884–2893 (2010).

12. H. Takesue, and K. Inoue, "1.5-μm band quantum-correlated photon pair generation in dispersion-shifted fiber: suppression of noise photons by cooling fiber," Opt. Express **13,** 7832–7839 (2005).
13. H. J. McGuinness, M. G. Raymer, C. J. McKinstrie, and S. Radic, "Quantum frequency translation of single-photon states in a photonic crystal fiber," Phys. Rev. Lett. **105,** 093604 (2010).
14. A. Farsi, S. Clemmen, S. Ramelow, and A. L. Gaeta, "Low-Noise Quantum Frequency Translation of Single Photons," in Conference on Lasers and Electro-Optics, OSA Technical Digest (2015) (Optical Society of America, 2015), paper FM3A.4.
15. C. J. McKinstrie, L. Mejling, M. G. Raymer, and K. Rottwitt, "Quantum-state-preserving optical frequency conversion and pulse reshaping by four-wave mixing," Phys. Rev. A, **85**, 53829 (2012).
16. M. Liscidini, J. E. Sipe, and L. G. Helt, "Continuous wave photon pair generation in silicon-on-insultator waveguides and ring resonators," Opt. Express **24,** 16558–16570 (2009).
17. C. Xiong, G. D. Marshall, A. Peruzzo, M. Lobino, A. S. Clark, D.-Y. Choi, S. J. Madden, C. M. Natarajan, M. G. Tanner, R. H. Hadfield, S. N. Dorenbos, T. Zijlstra, V. Zwiller, M. G. Thompson, J. G. Rarity, M. J. Steel, B. Luther-Davies, B. J. Eggleton, J. L. O'Brien, "Generation of correlated photon pairs in a chalcogenide As_2S_3 waveguide," Appl. Phys. Lett. **98,** 051101 (2011).
18. M. J. Collins, A. S. Clark, J. He, D.-Y. Choi, R. J. Williams, A. C. Judge, S. J. Madden, M. J. Withford, M. J. Steel, B. Luther-Davies, C. Xiong, and B. J. Eggleton, "Low Raman-noise correlated photon-pair generation in a dispersion-engineered chalcogenide As_2S_3 planar waveguide'," Opt. Lett. **37,.** 3393–3395 (2012).
19. I. Agha, M. Davanço, B. Thurston, and K. Srinivasan, "Low-noise chip-based frequency conversion by four-wave-mixing Bragg scattering in SiN_x waveguides," Opt. Lett. **37**, 2997–2999 (2012).
20. Y. Zhao, D. Lombardo, J. Mathews, and I. Agha, "Low control-power wavelength conversion on a silicon chip," Opt. Lett. **41**, 3651–3654 (2016).
21. B. A. Bell, J. He, C. Xiong, and B. J. Eggleton, "Frequency conversion in silicon in the single photon regime," Opt. Express **24**, 5235–5242 (2016).
22. S. M. M. Friis, Y. Jung, I. Begleris, P. Horak, K. Rottwitt, P. Petropoulos, D. J. Richardson, and F. Parmigiani, "Detailed phase matching characterization of inter-modal four-wave mixing in a two-mode fiber," in Conference on Lasers and Electro-Optics, OSA Technical Digest (2016) (Optical Society of America, 2016), paper JTu5A.49.
23. F. Parmigiani, Y. Jung, S. M. M. Friis, Q. Kang, I. Begleris, P. Horak, P. Petropoulos, K. Rottwitt, and D. J. Richardson, "Study of inter-modal four wave mixing in two few-mode fibres with different phase matching properties," in *Proceedings of European Conference on Optical Communication*, Tu2D.4 (2016).
24. C. J. McKinstrie, S. Radic, and A. R. Chraplyvy, "Parametric amplifiers driven by two pump waves," IEEE J. Sel. Top. Quantum Electron. **8,** 538–547 (2002).
25. Y. Xiao, R.-J. Essiambre, M. Desgroseilliers, A. M. Tulino, R. Ryf, S. Mumtaz, and G. P. Agrawal, "Theory of intermodal four-wave mixing with random linear mode coupling in few-mode fibers", Opt. Express **22,** 32039–32059 (2014).
26. F. Poletti and P. Horak, "Description of ultrashort pulse propagation in multimode optical fibers," J. Opt. Soc. Am. B **25,** 1645–1654 (2008).
27. J. Cheng, M. E. V. Pedersen, K. Wang, C. Xu, L. Grüner-Nielsen, and D. Jakobsen, "Time-domain multimode dispersion measurement in a higher-order-mode fiber," Opt. Lett. **37,** 347–349 (2012).
28. I.Kaminow, and T. Li, *Optical Fiber Telecommunications IV-B: Systems and Impairments* (Elsevier Science, 2002).
29. G. P. Agrawal, *Nonlinear Fiber Optics* (Academic, 2007).
30. R. H. Stolen, E. P. Ippen, "Raman gain in glass optical waveguides," Appl. Phys. Lett. **22,** 276–278 (1973).

1. Introduction

In the 1970's, Roger H. Stolen *et al.* showed for the first time inter-modal (IM) four-wave mixing (FWM) in silica-based optical fibers at visible wavelengths by achieving phase matching between different guided higher order spatial modes [1]. This study was conducted in short cm-length fibers due to the substantial fiber non-uniformity in longer fiber lengths at that time, which drastically reduced the FWM efficiency. Today, however, km-long few-mode fibers of much higher uniformity and thus low mode coupling are commercially available [2]. For example, this has allowed the recent experimental verification of IM FWM in a 4.7-km long two-mode fiber (TMF) at communication wavelengths [3, 4] and mode conversion based on FWM [5], thus suggesting that IM FWM may become feasible for optical signal processing as was the case for single-mode fiber optical parametric processes more than two decades ago [6–8]. Compared to the single mode nonlinear platform, the multi-mode one opens up an extra (spatial) degree of freedom to the system and, thus, could be a very interesting potential

means for enhancing the performance of many ultra fast signal processing applications, namely parametric amplification and wavelength conversion. For example, the multi-mode platform relaxes the requirements of phase matching, thus alleviating trade-offs between broadband operation and low noise. Specifically, operating near the zero-dispersion wavelength of the fiber to achieve phase matching is not required by the multi-mode platform so reduced nonlinear signal cross talk is expected. Another limiting factor of efficient signal amplification or frequency conversion using FWM is excess noise contributions such as spontaneous Raman scattering [9, 10] and broad-band amplified spontaneous emission (ASE) from a high-power pump [11]. The impact of the latter can be reduced by efficient, narrow filtering of the pump, but spontaneous Raman scattering is difficult to avoid in single-mode operation because its bandwidths typically extend beyond the phase matching bandwidth of the FWM process. If the wave components of the FWM process are excited in different spatial modes, however, phase matching can be achieved for large wavelength separations because of the different propagation constants of each mode. The impacts of spontaneous Raman scattering and ASE from a high-power pump may therefore potentially be reduced to an insignificant level by tailoring the dispersion properties of the multi-mode fiber such that phase matching is achieved beyond the spectral bands of these noise sources. Moreover, in quantum communication science, FWM in fibers has been used to generate correlated photon pairs [12], and it generally enables frequency conversion of quantum states of light [15]. The latter has been demonstrated in both a photonic crystal fiber [13] and a dispersion-shifted highly nonlinear fiber [14] in single-mode operation, where phase matching was achieved beyond the Raman spectrum by careful dispersion engineering, however at the cost of intrinsically narrow bandwidths. This is one reason why other platforms such as silicon and chalcogenide (As_2S_3) glass waveguides have been explored of late [16–21]; while these platforms operate single-moded and are less affected by Raman scattering, they are however not easily integrated in fiber networks. IM FWM thus potentially enables key applications for future quantum communication networks in fully silica-fiber integrated schemes and, more general, highlights its potential to have impact in several different fields of optics.

In this paper, extending from our previous work [22, 23], we numerically and experimentally characterize the phase matching properties mainly in terms of efficiency and bandwidth of two FWM processes, phase conjugation (PC) and Bragg scattering (BS) [24], in a 1-km long two-mode graded index fiber at telecommunication wavelengths. Figures 1(a)–1(c) show three pump(s) and signal configurations to achieve the following FWM processes: Fig. 1(a) modulation instability (MI), Fig. 1(b) PC, and Fig. 1(c) BS. MI and PC are amplification processes where one degenerate pump, p, or two separate pumps, p and q, amplify the signal, s, and simultaneously generate the idler, i. BS is an energy exchange process where the two pumps drive the conversion of photons from the signal to the idler [24]. In our experiment, one pump p, and a signal, s, are launched into the LP_{01} mode of the fiber, and a second pump, q, is launched into the LP_{11} mode. The PC and BS idlers are generated in the LP_{11} mode at a wavelength determined by the energy conservation requirements of the PC and BS processes, respectively, while the MI idler is generated in the LP_{01} mode, again at the wavelength determined by energy conservation. These configurations have been studied theoretically in another TMF [25], where it was shown that the phase matching of both processes depends critically on the wavelength separation of the pumps, and that a larger signal bandwidth of phase matching is achievable for the BS than for the PC processes. In this paper, we confirm these predictions experimentally in a TMF and present numerical simulations which agree well with our experimental results.

2. Theory

The theory section is divided in two parts: firstly, the principle of the two-mode phase matching is explained in detail and, secondly, we present our modeling of IM FWM in a TMF using the

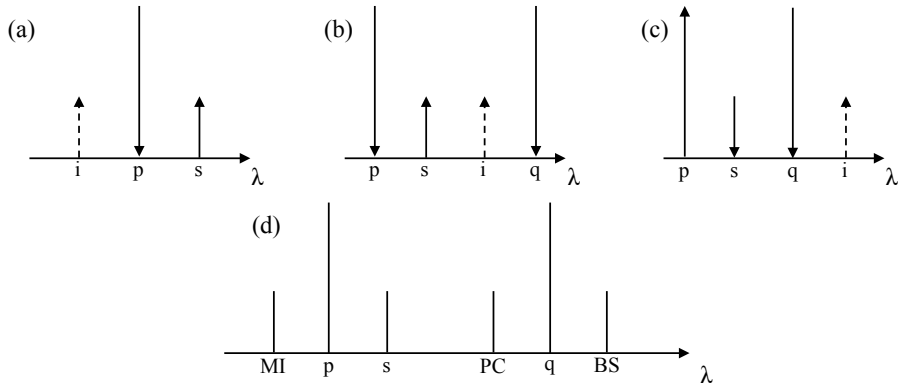

Fig. 1. Different configurations of FWM using two pumps, p and q, a signal, s, and an idler, i; (a) modulation instability (MI), (b) phase conjugation (PC), (c) Bragg scattering (BS) and (d) the full spectrum. The arrows indicate gaining (up) and losing (down) energy.

multi-mode generalized nonlinear Schrödinger equation (MM-GNLSE) [26].

2.1. Two-mode phase matching

The phase mismatch parameter, $\Delta\beta$, shown in Eq. (1), is calculated by expanding the wavenumber of each participating wave in a Taylor series around an arbitrary frequency ω_0, and we denote $\beta_k^{(\mu)}(\omega_0)$ as the k'th order expansion coefficient in the Taylor expansion of the wavenumbers for mode μ. The terms with $k=0$ cancel from $\Delta\beta$ [4], the terms with $k=1$ are the inverse group velocity (IGV), and the terms with $k=2$ represent the chromatic dispersion of mode LP_μ through $D^{(\mu)} = -(2\pi c/\lambda_0^2)\beta_2^{(\mu)}$, where $\lambda_0 = 2\pi c/\omega_0$. If it is assumed that pump p and signal s are in the LP_{01} mode and pump q and idler i are in the LP_{11} mode, the phase mismatch for the BS process becomes

$$\begin{aligned}\Delta\beta &= \beta(\omega_s) + \beta(\omega_q) - \beta(\omega_p) - \beta(\omega_i) \\ &\approx \left[\beta_1^{(01)} + \beta_2^{(01)}\left(\frac{\Delta\omega_s + \Delta\omega_p}{2}\right) - \beta_1^{(11)} - \beta_2^{(11)}\left(\frac{\Delta\omega_q + \Delta\omega_i}{2}\right)\right](\omega_s - \omega_p),\end{aligned} \tag{1}$$

where the wave numbers are expanded to the second order only and the mode designations $\mu = 01$ and $\mu = 11$ refer to the scalar modes LP_{01} and LP_{11} and $\Delta\omega_n = \omega_n - \omega_0$ for $n = p$, q, s, i. The first term in square brackets has also been reported in [4] and we also include the second term, $(\omega_s - \omega_p)$, as it is important to fully understand our results. From Eq. (1) the phase mismatch becomes small when the IGV of each mode evaluated at the average wavelength of the waves in the same mode are nearly equal [4]. This means that the IGV at the average wavelength of the signal s and pump p in the LP_{01} mode has to lie on the same horizontal line as the IGV of the average wavelength of the idler i and pump q in the LP_{11} mode, see Fig. 2(a), where the BS process is illustrated. Note that if the wavenumbers in Eq. (1) are expanded to higher orders in frequency, other solutions to the phase matching condition that do not share the graphical interpretation of Fig. 2(a) may appear at larger wavelength separations.

For the BS case, phase matching can be perfectly conserved when tuning the signal wavelength if the two IGV lines are parallel (same dispersion) and without curvature (negligible dispersion slope). This property is due to its corresponding energy conservation that causes the idler wavelength to change in the same way as the signal wavelength. On the other hand, for the PC process (obtained by exchanging q and i in Eq. (1) and Fig. 2(a)), the same property

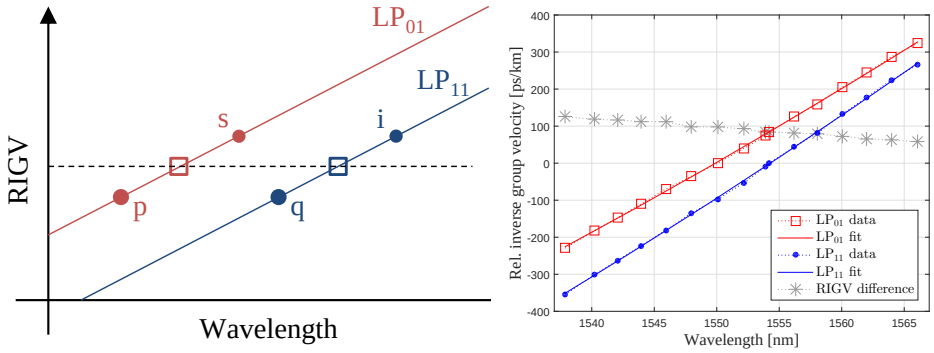

(a) (b)

Fig. 2. (a) Principle of two-mode phase matching for distant BS in a RIGV vs. wavelength diagram; dots denote wave components and squares denote the average wavelength of the two waves in either mode. (b) RIGV measurements of LP_{01} and LP_{11} vs. wavelength; lines denote second order polynomial fits and the grey stars denote the inverse group velocity difference.

does not hold: the signal and idler wavelengths move in opposite directions to fulfill energy conservation. Thus only at one signal wavelength (relative to p) phase matching is perfectly fulfilled. This is the reasoning behind the different bandwidths of the two processes. Finally, note in Eq. (1) that the last term also makes the phase mismatch vanish when $\omega_s = \omega_p$ (and consequently $\omega_i = \omega_q$), which follows trivially from the consideration that in this case when two photons are annihilated, the two new photons are generated in the same modes and at the same wavelengths.

Figure 2(b) shows the measured relative IGV (RIGV) versus wavelength of the LP_{01} (red) and LP_{11} (blue) modes in our TMF using time-of-flight measurements [27]. As can be extracted from the figure, phase matching can be fulfilled for a pump-to-pump detuning of about $\Delta\lambda = 4.4$ nm and the RIGV lines of the two modes are separated by ~ 98 ps/km from each other at $\lambda_0 = 1550$ nm. Second order polynomials were fitted to each data set to find the chromatic dispersions of the two modes, and we find $D^{(01)} = 19.8$ ps/(km nm) and $D^{(11)} = 21.8$ ps/(km nm), in good agreement with the simulated data sheet values for this fiber of $D^{(01)}_{\text{sim}} = 19.9$ ps/ (km nm) and $D^{(11)}_{\text{sim}} = 22.1$ ps/(km nm). While Eq. (1) neglected $\beta_3^{(\mu)}$, in our particular case it was found to influence the conversion efficiency to a small degree for larger signal-to-pump wavelength detunings and thus we include its effect in the simulations described below. In particular, we consider a dispersion slope $S^{(01)} = 0.068$ ps/(km nm^2) and $S^{(11)} = 0.063$ ps/(km nm^2). The third order Taylor expansion coefficients for mode μ are calculated using $\beta_3^{(\mu)} = (\lambda_0/2\pi c)^2 (2\lambda_0 D^{(\mu)} + \lambda_0^2 S^{(\mu)})$ [28].

2.2. *Simulations*

FWM processes can be predicted simply by solving the coupled amplitude equations [29]. However, in our case multiple and cascaded FWM processes occur, so each generated idler is the result of several of these effects. For example the BS idler is a result of process (b) in Fig. 1 but is also affected by IM-FWM of the pumps and the MI idler amongst others.

In order to encompass all possible interactions, the system is solved using the MM-GNLSE [26]. The dynamics of the amplitude of mode μ propagating along the z direction is determined by the sum of the mode dispersion ($\mathscr{D}_\mu$) and the nonlinear ($\mathscr{N}_\mu$) terms:

$$\frac{\partial A_\mu(z,t)}{\partial z} = \mathscr{D}_\mu(z,t) + \mathscr{N}_\mu(z,t), \tag{2}$$

where the dispersion and nonlinear term are described by

$$\mathscr{D}_\mu(z,t) = \left(j\left(\beta_0^{(\mu)} - \beta_0^{(01)}\right) - \left(\beta_1^{(\mu)} - \beta_1^{(01)}\right)\frac{\partial}{\partial t} - j\frac{\beta_2^{(\mu)}}{2}\frac{\partial^2}{\partial t^2} + \frac{\beta_3^{(\mu)}}{6}\frac{\partial^3}{\partial t^3} \right) A_\mu(z,t), \tag{3}$$

$$\begin{aligned} \mathscr{N}_\mu(z,t) = j\frac{n_2\tilde{\omega}}{c}\sum_{l,m,n}\left(1+\frac{j}{\omega_0}\frac{\partial}{\partial t}\right) Q_{\mu lmn} A_l(z,t)\Bigg(& 3(1-f_R)A_m(z,t)A_n^*(z,t) \\ & +3f_R\int h(\tau)A_m(z,t-\tau)A_n^*(z,t-\tau)d\tau \Bigg) \end{aligned} \tag{4}$$

respectively. Here, f_R is the fractional contribution of the Raman response to the Kerr effect, $h(\tau)$ the delayed Raman response function, n_2 is the nonlinear refractive index, $\tilde{\omega}$ is a reference frequency of the spectrum and $Q_{\mu lmn}$ are the overlap integrals defined in [26].

In our model, the input wave components were simulated as continuous waves (CWs), which are represented as delta functions in wavelength space. The reference frequency $\tilde{\omega}$ of the spectrum was taken to be that of the LP_{01} pump and then the minimum and maximum wavelengths of the spectral window used in the simulations were chosen to include all input and output wavelengths. Two waves, p and s, are launched in the LP_{01} mode and one wave, q, is launched in one of the two degenerate LP_{11} modes (e.g. in the LP_{11a} mode). The LP_{01} and LP_{11} amplitudes are then propagated through the 1-km TMF by solving Eq. (2) using a symmetrized split step Fourier method.

The TMF is a silica fiber and hence we set $n_2 = 2.5\cdot10^{-20}$ m^2 W^{-1}, $f_R = 0.18$, and $h(\tau)$ is calculated using the measured curve shown in [30]. For each of the indices of $Q_{\mu lmn}$, zero represents the LP_{01} mode and unity the LP_{11} mode. For the case where the indices are equal the overlaps were found to take the values of $Q_{0000} = 2.07\cdot10^9$ m^{-2} and $Q_{1111} = 1.96\cdot10^9$ m^{-2} respectively. Due to the symmetry between the LP_{01} and one of the degenerate LP_{11} modes considered here, all the overlaps which have an equal and even number of ones and zeros as indices are equal and were found to be $Q_e = 1.28\cdot10^9$ m^{-2} while all other overlap factors vanish.

The output spectrum, see Fig. 1(d), was used to calculate the conversion efficiency (CE) of the processes of interest, which we have defined as the ratio of the output idler and signal powers for both the PC and BS processes. This CE definition is justified by the difficulty of accurately measuring the input signal power and the relatively small generated idlers, highlighting that the system is far from high gain operation for which the CE limit of PC is 0 dB and the maximum CE for BS is infinity.

Figure 3 presents the CE for both the PC and BS processes for varying signal and pump q wavelengths at a constant pump wavelength, $\lambda_p = 1549$ nm. The CE is primarily dependent upon the phase mismatch parameter. High CEs are achieved for both processes when λ_s is close to λ_p as a result of the last term of Eq. (1). However, very different behavior is observed for the two processes moving away from this condition. The CE of the PC process remains high if λ_s and λ_q are simultaneously changed. On the other hand, the CE of the BS process remains high for a large λ_s detuning for a relatively constant λ_q. From Fig. 2(a) and Eq. (1) it is clear that arbitrarily large CE bandwidth for an optimized (fixed) pump q wavelength can be achieved if the RIGV curves of the two modes are parallel, i.e. both modes have the same dispersion coefficient D and vanishing dispersion slope S. For non-identical dispersion, as measured for

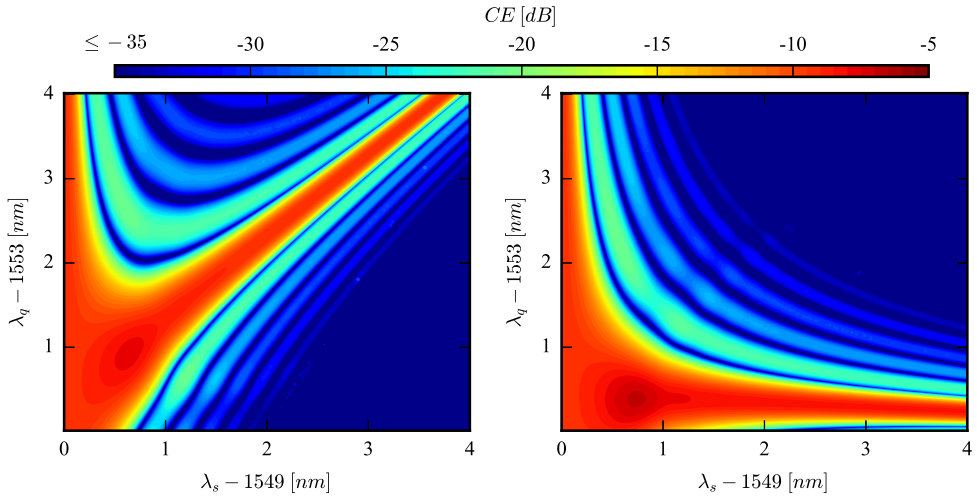

Fig. 3. Conversion efficiency of the PC (left) and BS (right) for a variation of signal and pump q wavelengths. $\lambda_p = 1549$ nm and input powers are $P_p = P_q = 27.5$ dBm, $P_s = 3.5$ dBm.

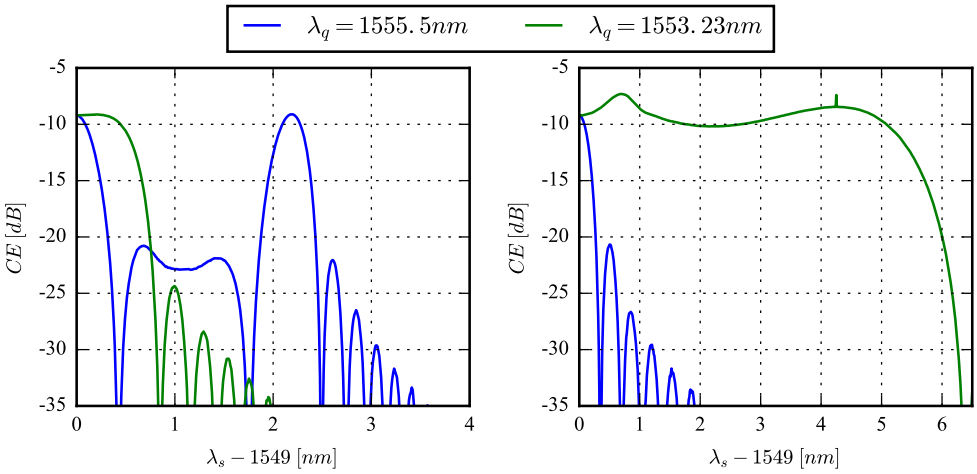

Fig. 4. Conversion efficiency of the PC (left) and BS (right) for selected λ_q shown in the legend. The paramaters are the same as in Fig. 3.

our fiber, see Fig. 2(b), a change in signal wavelength also requires a small change in pump q wavelength to maintain perfect phase matching. This required change of λ_q depends on the difference in dispersion between the two modes and follows linearly the change of the signal wavelength, thus leading to a slight tilt of the perfectly phase matched region at the bottom of Fig. 3(b). This therefore limits the achievable signal bandwidth for fixed λ_q. Moreover, for non-vanishing dispersion slope S, which manifests itself as a curvature of the RIGV curves in Fig. 2, a term that is nonlinear in the signal wavelength enters the phase matching equation. This term becomes important for large wavelength differences between waves p and q, and between waves p and s, and leads to a curvature of the perfectly phase matched region at the bottom of

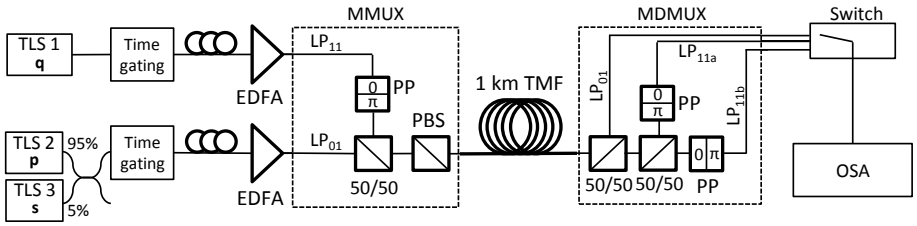

Fig. 5. Sketch of the experimental setup. TLS, tunable laser source; MMUX, mode-multiplexer; EDFA, Erbium-doped fiber amplifier; 50/50, 3-dB non-polarization beam-splitter; PBS, polarization beam-splitter; PP, phase plate; TMF, two-mode fiber; MDMUX, mode-demultiplexer; OSA, optical spectrum analyzer.

Fig. 3(b) which again affects the achievable bandwidth at fixed λ_q.

For clarity, two cross sections of Fig. 3 are also shown in Fig. 4 for $\lambda_q = 1553.23$ nm and $\lambda_q = 1555.5$ nm respectively. At the optimum pump wavelength for BS ($\lambda_q = 1553.23$ nm) the bandwidth extends to ≈ 5 nm at -3 dB whereas the PC one is limited to < 0.5 nm at -3 dB. For the longer pump q wavelength in Fig. 4, the PC CE shows two peaks of similar height separated by ≈ 2.3 nm whereas the BS bandwidth has become very narrow (≈ 0.2 nm).

Particularly for the BS process a maximum can be observed at a signal-to-pump detuning of ≈ 0.7 nm and this is attributed to the influence of the MI process adding to the output idler. Moreover the pumps p and q can also interact with each other without the signal, which results in idlers found at frequencies $2\omega_p - \omega_q$ and $2\omega_q - \omega_p$. In the special case $\lambda_s = \lambda_q$, all of MI, PC, and BS as well as the direct pump-pump interactions fall on the same set of frequencies, so the idlers produced by the pump-pump interactions add coherently to the PC and BS idlers. In our example, this effect appears as a slight increase in the BS CE in Fig. 4 for $\lambda_s = \lambda_q = 1553.23$ nm.

3. Experimental setup for inter-modal four-wave mixing characterization

The experimental setup for measuring and characterizing IM FWM of the TMF discussed in the previous sections is shown in Fig. 5. Three tunable laser sources are used to generate the inputs, i.e. pump p (TLS 2), pump q (TLS 1), and signal s (TLS 3), and a 95/5 coupler is used to achieve about 22 dB power difference between p and s. All inputs are time gated with a 10% duty cycle and a repetition rate of 10 MHz to avoid stimulated Brillouin scattering and to increase the peak powers. Two polarization controllers are used to co-polarize the waves in the LP_{01} and LP_{11} optical paths, respectively, which is ensured by the polarization beam-splitter (PBS) after beam combination in the 50/50 non-polarization beam-splitter. Single mode Erbium-doped fiber amplifiers (EDFAs) amplify the inputs to achieve an average power of 20.5 dBm in each pump at the TMF output; the loss of the fiber was verified to be $\sim$0.2 dB/km in both modes.

The first pump p and signal s are launched into the LP_{01} mode while the second pump q is launched into the LP_{11} mode using a mode-multiplexer (MMUX) based on a phase plate (PP), which shifts the phase of half the beam front in the transverse plane by π. The launching mode purity was -28 dB between LP_{01} and LP_{11}, while the mode degeneracy of the LP_{11} mode induces strong linear coupling between the LP_{11a} and LP_{11b} modes.

A mode-demultiplexer (MDMUX) based on PPs and single mode fibers (SMFs) was used to separate each spatial mode using two 3-dB beam splitters as shown in Fig. 5. The first component of the split beam is used to measure the power in the LP_{01} mode of the TMF by coupling

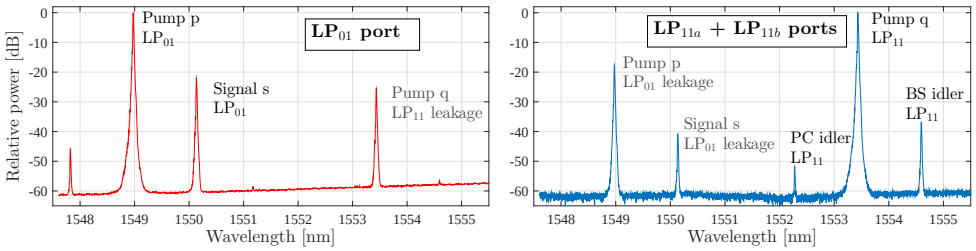

Fig. 6. Performance of the MDMUX; the LP_{01} port (left) extinguishes the LP_{11} mode by 25 dB, and the LP_{11} port (right) extinguishes the LP_{01} mode by 18 dB.

Table 1. Pump q wavelengths used in experiments; pump p is $\lambda_p = 1549$ nm in all cases.

	λ_q [nm]	λ_q - λ_p [nm]		λ_q [nm]	λ_q - λ_p [nm]
(a)	1553.00	4.00	(d)	1553.75	4.75
(b)	1553.40	4.40	(e)	1554.50	5.50
(c)	1553.5	4.50	(f)	1554.70	5.70

directly into a SMF without allowing the content of the LP_{11} mode to propagate. Due to the strong linear mixing between LP_{11a} and LP_{11b} both the LP_{11} mode demultiplexed output ports need to be used to collect all of the signal power launched into the initial LP_{11a} mode. In particular, two orthogonal PPs are used to convert the LP_{11a} and LP_{11b} modes back to the LP_{01} mode, so that it can be properly collected by the following SMFs.

Figure 6 shows the optical spectra at the LP_{01} output port (left) and the sum of two spectra obtained in each of the two LP_{11} output ports (right) for a typical measurement where the wavelengths of the input LP_{01} pump p, signal s, and LP_{11} pump q were $\lambda_p^{(01)} = 1549$ nm, $\lambda_s^{(01)} = 1550.15$ nm, and $\lambda_q^{(11)} = 1553.45$ nm, respectively. The data is normalized to the LP_{01} and LP_{11} pump output powers (assumed to be equal) in each graph, respectively. The spectrum at the LP_{01} output port clearly highlights the intra-modal MI FWM process of Fig. 1(a); the combined spectra in the LP_{11} output ports show the PC and BS IM-FWM processes of Figs. 1(b) and 1(c). From the graphs it can be observed that the LP_{01} port extinguishes the LP_{11} mode by 25 dB while the LP_{11} port extinguishes the LP_{01} mode by 18 dB.

4. Experimental results and discussion

We experimentally characterized the phase matching properties of the two different IM FWM processes. Considering Fig. 3 we chose to experimentally investigate both PC and BS processes using a pump p wavelength of $\lambda_p = 1549$ nm and six pump q wavelengths, each of them showing different characteristics in terms of CE versus signal wavelengths. The corresponding wavelengths along with the pump separations are shown in Table 1 as cases (a)–(f). For each value of λ_q the signal wavelength was scanned and for every iteration a spectrum was saved on the OSA. The collection of a complete set of signal wavelength lasts approximately one hour during which time the MMUX and MDMUX are stable.

Figure 7 plots the measured CE of the PC process with respect to the signal wavelength for all the above choices of pump q wavelengths, i.e. cases (a)–(f). As predicted above, the measured CE has different characteristics (vs. signal wavelength) for values below and above $\lambda_q \approx 1554$ nm. For $\lambda_q < 1554$ nm (cases (a) and (b)) the CE has only one peak and its width

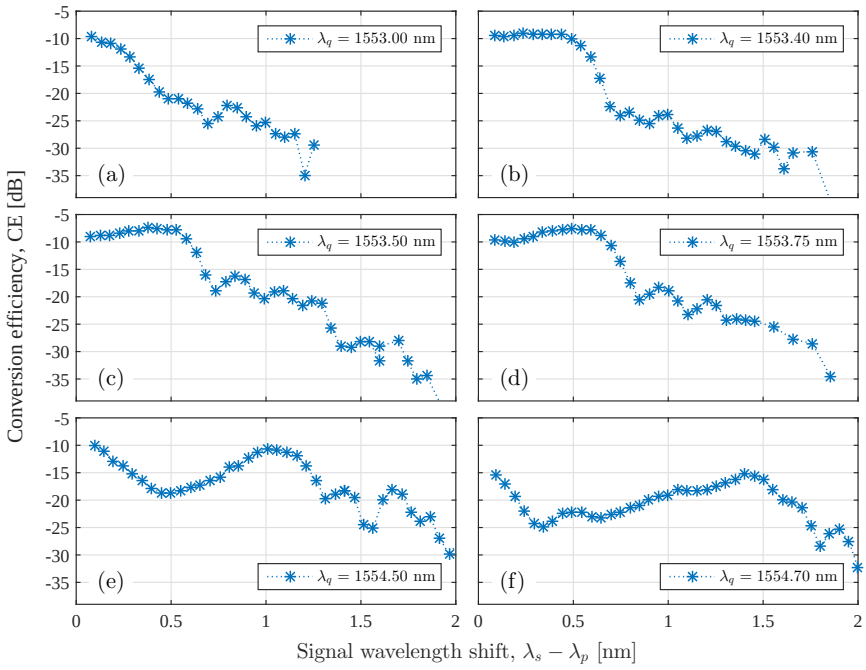

Fig. 7. Measured conversion efficiency for PC vs. signal wavelength for cases (a)–(f) of pump q wavelengths corresponding to the values given in Table 1.

increases with λ_q from 0.25 nm to 0.75 nm in accordance with the results shown in Fig. 3. This peak, close to $\lambda_s - \lambda_p = 0$, is present due to PC being phase matched because the $(\omega_s - \omega_p)$-term in Eq. (1) is small. In case (d), we observe that the single phase matching peak is starting to split up into two peaks. For $\lambda_q > 1554$ nm (cases (e) and (f)) the CE presents two clearly separated peaks and their separation increases with larger λ_q. The other peak is present when the first term in square brackets in Eq. (1) is small. The highest CE is found in case (c) where a CE of -7.4 dB is achieved at $\lambda_s - \lambda_p \approx 0.5$ nm due to the cascaded FWM processes discussed in the simulation section.

Figure 8 plots the CE of the BS process as a function of wavelengths for the same operating conditions used to obtain Fig. 7. As predicted in the simulation section, only in a narrow interval of pump q wavelengths, close to $\lambda_q \approx 1553.5$ nm (cases (b) and (c)), the phase matching bandwidth reaches about 1.2 nm at -3 dB, which is wider than any bandwidth observable in the PC process. Case (a) with $\lambda_q < 1553.5$ nm has a narrow bandwidth (about 0.7 nm) compared to cases (b) and (c), which have pump q wavelengths inside the phase matching region, as predicted by Fig. 3. The maxima around $\lambda_s - \lambda_p = 0.5$ nm in (b) and (c) are also predicted by theory and are a result of a combination of different cascade FWM processes. The pump q wavelength of case (d) lies on the upper edge of the phase matching region of Fig. 3, and indeed its bandwidth diminishes. Cases (e) and (f) are well above the region of phase matching so the CE bandwidth reduces to 0.2 nm at -3 dB for case (f). The highest CE of -6.3 dB is found in case (b) where again BS is enhanced by further cascaded FWM processes. Higher CE for both PC and BS can be achieved by increasing the pump powers further and by using a fiber with a higher nonlinearity.

As is evident from Fig. 3, the conditions for phase matching are highly sensitive to the dispersion properties of the fiber and most importantly its relative mode dispersion. For the PC

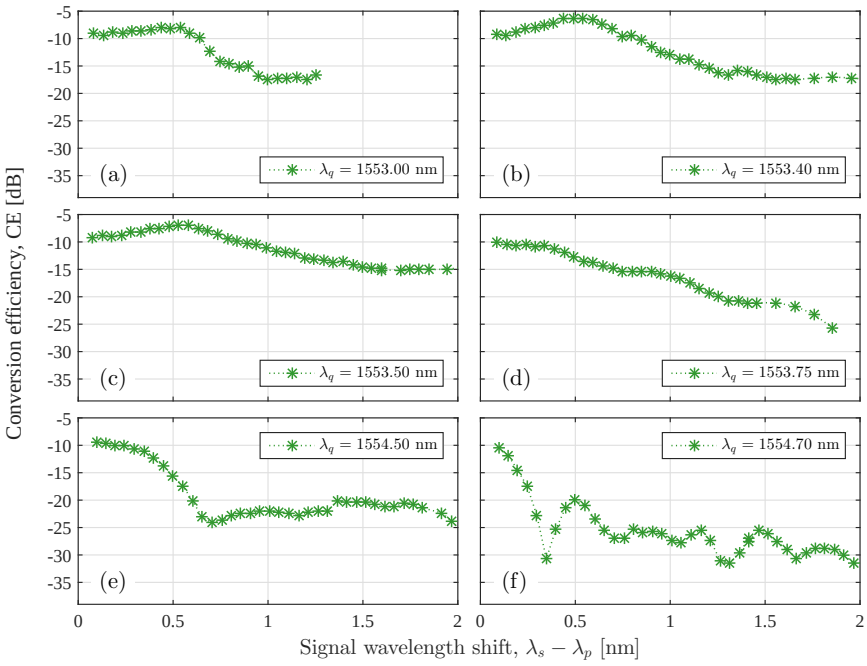

Fig. 8. Measured conversion efficiency for BS vs. signal wavelength for cases (a)–(f) of pump q wavelengths corresponding to the values given in Table 1.

process, phase matching can be achieved for a relatively wide range of pump q wavelengths but at any given value the bandwidth of phase matching of the signal is very narrow at only ~ 0.3 nm. In the BS process, phase matching is achievable only in a very narrow interval of pump q wavelengths; however its corresponding bandwidth can potentially be very broad, depending on the dispersion properties of the phase matched modes. Clearly, any fabrication imperfections that cause fluctuations along the fiber length in the relative dispersion parameters among the various modes, such as inverse group velocity, dispersion coefficient, or dispersion slope, lead to critical changes in the phase matching condition of the IM-FWM. Thus, one must expect that any experimental investigation that tries to map out the conversion efficiency in Fig. 3 finds a more blurred picture with broader and lower amplitude features particularly for the BS process when relative long fibers are used, such as in our work here. Shorter fiber lengths could avoid this issue and potentially allow broader CE to be observed, as predicted in the simulations.

To avoid ASE noise from a high-power pump and Raman scattering in ultra-fast optical signal processing using the multi-mode platform, as outlined in the introduction, phase matching at larger wavelength separations than demonstrated in this work must be achieved. One solution in the case of using only two modes is separating the signal and idler in Fig. 2(a) more than the width of the Raman peak of 100 nm (at telecommunication wavelengths) from the two pumps; due to filtering the pump before the fiber input, ASE noise is likely to be spectrally narrower than Raman scattering. The signal-to-idler wavelength separation can be controlled through dispersion engineering of the fiber by changing the separation of the IGV curves of the two modes. In this case, however, the phase matching condition becomes more complicated than Eq. (1) because each wavenumber must be expanded to higher than second order. Using three or four modes is possible given non-zero overlap integrals but it changes the phase matching

condition completely from the picture described in this paper.

5. Conclusion

We characterized the phase matching properties of two separate inter-modal four-wave mixing processes, phase conjugation and Bragg scattering, in a 1-km long two-mode fiber. The experimental results, which show good qualitative agreement with the simulations, highlight the potential of Bragg scattering as a broadband process in phase matched and dispersion tailored few-mode fibers. For the investigated two-mode fiber the simulation predicted a conversion efficiency bandwidth of the Bragg scattering process of 5 nm while a bandwidth of 1.2 nm was measured. We believe that this discrepancy is caused by fluctuations of the modal dispersion along the fiber length and much larger bandwidths are expected to be measured moving to shortened (and more nonlinear) fiber lengths.

Funding

UK Engineering and Physical Sciences Research Council (EPSRC) (EP/I01196X, The Photonics Hyperhighway); EPSRC Centre for Doctoral Training in Next Generation Computational Modelling (EP/L015382/1); Danish Council for Independent Research (DFF) (4184-00433). Dr. F. Parmigiani is supported by a Royal Academy of Engineering/EPSRC research fellowship.

Acknowledgment

The authors acknowledge the use of the IRIDIS High Performance Computing Facility and associated support services at the University of Southampton in the completion of this work. The data used in this paper is openly available at: http://dx.doi.org/10.5258/SOTON/403696.